Thermal dissociation of alkyl nitrites and recombination of alkyl radicals

John B. Randazzo[1], Mark E. Fuller[2], C. Franklin Goldsmith[2], and Robert S. Tranter[1]

[1]*Chemical Sciences and Engineering Division, Argonne National Laboratory, 9700 S. Cass Avenue, Argonne, IL 60439, United States*
[2]*School of Engineering, Brown University, 184 Hope Street, Providence, RI 02912, United States*

Corresponding author: Robert S. Tranter
E-mail: tranter@anl.gov
Phone: +1-630-252-6505
Address:
Chemical Sciences and Engineering Division, Bldg 200
Argonne National Laboratory
Argonne, IL, USA 60439

This manuscript is accompanied by supplemental material with additional tables and figures.

Colloquium: Gas-Phase Reaction Kinetics

Colour figures online only. Greyscale in print

Word count: Method 1
Text: 3080
References: (47+2)*2.3*7.6 = 857
Table 1: (16+2)*7.6*1 = 144
Table 2: (5+2)*7.6*2 = 106
Figure 1: [(3.79*25.4)+10]*2.2*1+44 = 277
Figure 2: [(2.08*25.4)+10]*2.2*1+25 = 163
Figure 3: [(2.07*25.4)+10]*2.2*1+28 = 166
Figure 4: [(2.03*25.4)+10]*2.2*1+24 = 159
Figure 5: [(2.15*25.4)+10]*2.2*1+35 = 177
Figure 6: [(2.07*25.4)+10]*2.2*1+32 = 170
Figure 7: [(2.10*25.4)+10]*2.2*1+13 = 152
Figure 8: [(2.14*25.4)+10]*2.2*1+27 = 169
Figure 9: [(2.03*25.4)+10]*2.2*1+30 = 165

Total: 5787

Abstract

The thermal dissociations of three alkyl nitrites (propyl, n-butyl and i-butyl) have been studied in a diaphragmless shock tube by laser schlieren densitometry over 700< T<1000K and 60<P<240 Torr. The nitrites act as clean, thermal sources of alkyl radicals that create the radicals at much lower temperatures than are accessible with other precursors. The decomposition of the three nitrites proceeds via a common mechanism, which is discussed. Rate coefficients for dissociation of the alkyl nitrites to an alkoxy radical and NO, k_1, were obtained with an uncertainty of 30%. Rice-Ramsperger-Kassel-Marcus/Master Equation (RRKM/ME) calculations for dissociation of the nitrites were performed and provide excellent simulations of the experimental results. The high-pressure limit rate coefficients from the RRKM/ME calculations are: $k_{1,C3H7ONO} = (5.69\pm1.71)\times10^{21}T^{-1.60}\exp(-21458/T)\ s^{-1}$; $k_{1,n\text{-}C4H9ONO} = (9.91\pm2.97)\times10^{21}T^{-1.59}\exp(-21588/T)\ s^{-1}$; $k_{1,i\text{-}C4H9ONO} = (3.92\pm1.18)\times10^{21}T^{-1.58}\exp(-21162/T)\ s^{-1}$. At the low temperatures of this work, the alkyl radicals are thermally stable and thus their recombination reactions were also studied. The recombination rate coefficients for ethyl, n-propyl and i-propyl radicals (uncertainties of 50%) are in excellent agreement with literature values, particularly recent theoretical results, and extend the range of experiments to higher temperatures.

Keywords: Shock tube; nitrite; radical source; radical recombination

1. Introduction

The critical steps in hydrocarbon oxidation and pyrolysis are dominated by reactions of organic radicals. Experimental study of the reactions of radicals requires clean sources of the radicals that can be used over a broad range of conditions. Radicals are often generated by pyrolysis of precursors, e.g. in shock tube experiments, but because of the high activation barriers to decomposition these sources are typically limited to relatively high temperatures. Organic nitrites, RO-NO ($R>CH_3$), are an underexploited, clean, thermal source of radicals that have considerable potential for high temperature chemical kinetic studies. For instance, using thermal decomposition of 3-methyl-but-3-enyl nitrite as a source of an alkenyl radical Tranter et al. [1] studied the recombination 2-methylally radicals in the low temperature oxidation regime where the reaction is important to ignition of i-butene. In the current work, the focus is on characterizing alkyl nitrites as sources of alkyl radicals and the subsequent reactions of the radicals. Reaction conditions were selected to allow the initial kinetics and mechanisms to be accurately determined. The experiments were conducted in a diaphragmless shock tube (DFST) by laser schlieren densitometry (LS) using the same techniques as Ref. [1]. Three alkyl nitrites (C_3H_7ONO, n-C_4H_9ONO, i-C_4H_9ONO) were studied over a broad range of conditions ($700<T<1000$ K; $60<P<250$ Torr). The alkyl radicals produced are thermally stable over most of the experimental range. Thus, the secondary chemistry is dominated by recombination and disproportionation reactions and rate coefficients were also obtained for these processes at temperatures where there is little or no experimental data. The experimental work was complemented by a theoretical study in which Rice-Ramsperger-Kassel-Marcus/Master Equation (RRKM/ME) calculations were performed for dissociation of the nitrites. The results of these calculations facilitate the use of the nitrites as radical sources at temperatures and pressures outside the range of this work.

Table 1: Generic mechanism for decomposition of alkyl nitrites

#	Rxn	$\Delta H_{r,298K}$[a]
1	$R\text{-}CH_2\text{-}O\text{-}NO = R\text{-}CH_2\text{-}O + NO$	41.9±0.6
2	$R\text{-}CH_2O = R + CH_2O$	11.3±0.3
3	$R = CH_3$ + alkene	23.3
4	R = H + alkene	34.4±1.7
5	R + R = RR	-86.8±1.6
6	$R + R = R_{-H} + RH$	-66.0±2.7
7	R + H = RH	-100.0±1.3
8	$R + H = R_{-H} + H_2$	-69.9±1.7
9	$R + CH_3 = RCH_3$	-89.3
10	$CH_3 + CH_3$ C_2H_6	-90.0

[a] $\Delta H_{r,298K}$ are averaged from $R=C_2H_5$, $n\text{-}C_3H_7$ and $i\text{-}C_3H_7$. See Table S1 for $\Delta H_{r,298K}$ for specific reactions.

The decomposition of the alkyl nitrites presented here ($R\text{-}CH_2O\text{-}NO$) and reactions of the alkyl radicals (R) follow a common set of reactions, Table 1. The initial step is scission of the weak O-NO bond to form an oxy radical ($R\text{-}CH_2O$) and NO. For C1-C4 alkyl nitrites Batt et al. [2] determined the O-NO bond energy to be ~41±1.5 kcal/mol. The next weakest bond is C-ONO, ~60 kcal/mol [1,2] and at the low temperatures of this work breaking this bond will be uncompetitive with loss of an NO group. Thus the alkyl nitrites decompose solely by loss of NO. In the nitrites studied here, the O-atom in the oxy radical is attached to a CH_2 group, and elimination of formaldehyde from $R\text{-}CH_2O$ is facile. The net result of the first two reactions in Table 1 is that decomposition of $R\text{-}CH_2O\text{-}NO$ yields a radical, R, with one less C-atom than the nitrite and H_2CO and NO. Under many conditions H_2CO and NO are effectively unreactive, particularly in oxygen free environments, and the alkyl nitrites are a clean source of alkyl radicals.

2. Methods

2.1. Experimental

The DFST [3,4] and LS technique [5,6] are described in detail elsewhere. The DFST creates reproducible shock waves with well-controlled, predictable properties. The temperatures, T_2, and pressures, P_2, behind the incident shock are calculated from the shock velocity and loading conditions assuming frozen conditions. The shock velocities were obtained from the time taken for the shock to pass between pressure transducers centered around the observation point. The uncertainty in velocity is estimated as 0.2% (i.e., 4-6 K in T_2).

LS measurements were made behind incident shock waves by measuring the deflection of a narrow laser beam, which is directed across the shock tube perpendicular to the direction of propagation of the shock wave. The time-resolved angular deflection is dependent on the molar refractivity of the mixture, the shock tube width, and the axial density gradients, $d\rho/dx$, in the shock-heated gases resulting from chemical reactions [5,6]. The molar refractivity of Kr is 6.367 $cm^3\ mol^{-1}$ [7]. The molar refractivity of each nitrite was calculated by the Lorenz-Lorentz equation [7], giving C_3H_7ONO=21.800 cm^3mol^{-1}, n-C_4H_9ONO=26.828 cm^3mol^{-1}, and i-C_4H_9ONO=27.004 cm^3mol^{-1}. The measured $d\rho/dx$ is related to the chemical reactions by $d\rho/dx \propto \Sigma r_i\ (\Delta H_{r,i} - C_pT\Delta N_i)$ [5,6] (r = rate of reaction, ΔH_r = enthalpy of reaction, C_p = mixture heat capacity, T = temperature, and ΔN = change in mole number). In general, $r_j\Delta H_j$ dominates and thus the density gradient is most sensitive to reactions that have a high rate of reaction and/or large absolute enthalpy of reaction. The normal assumption was made that the mixture molar refractivity does not change appreciably during reaction. This is an excellent assumption for dilute mixtures such as used here. For instance, in an experiment with 2% i-C_4H_9ONO/Kr, T_2= 999 K and P_2 = 60 Torr, the mixture refractivity varied by 4% after 10 μs, which has a negligible effect on the derived density gradient.

n-Butyl nitrite and iso-butyl nitrite were purchased from Sigma Aldrich and n-propyl nitrite was synthesized following Ref. [1], and the identity and purity was confirmed by infrared spectroscopy, ^1H

NMR, and ^{13}C NMR (Figs. S1-S5, and synthesis method, supplemental material). Prior to use, the nitrites were degassed by repeated freeze-pump-thaw cycles using liquid nitrogen. Mixtures of 0.5%, 1% or 2% of each alkyl nitrite dilute in krypton were prepared manometrically in an evacuated 50 L glass vessel and stirred until well mixed.

2.2. Theory

The C_3H_7ONO and C_4H_9ONO potential energy surfaces (PES) were computed using M11/jun-cc-pVTZ [8]. This same method was used for methyl nitrite and was compared against benchmark methods obtained using ANL0 [9]. For methyl nitrite, the DFT method was found to under predict the bond-dissociation energy (BDE) by 2.2 kcal/mol. Consequently, the BDE for the n-propyl nitrite, n-butyl nitrite and iso-butyl nitrite were shifted by 2.2 kcal/mol to 40.6, 40.8 and 40.1 kcal/mol, respectively. All DFT calculations were performed in GAUSSIAN09 [10].

The RRKM/ME calculations were performed using the program MESS [11], which is part of the PAPR package from Argonne National Laboratory [12]. A single exponential was used to model the collisional energy transfer, with $\langle \Delta E_{down} \rangle = 200\ (T/298)^{0.85}\ cm^{-1}$. For the O-N bond fission, a simple analytic model was used to describe the interaction potential, as implemented using the PhaseSpaceTheory keyword in MESS [13–15]. The coefficient of the interaction potential was adjusted so that the high-pressure limit of the reverse reaction had a rate coefficient of approximately 3×10^{-11} $cm^3molecule^{-1}s^{-1}$, based upon analogy for other radical + NO reactions [16].

Table 2. Experimental conditions for each of the nitrite species investigated in this study.

Species (# Shocks)	T_2/K	P_2/Torr	Concentration (in Kr)
n-propyl nitrite (60)	720-943	65, 120, 250	0.25%, 0.5%, 1%, 2%
n-butyl nitrite (40)	693-940	65, 135, 250	0.5%, 1%, 2%
iso-butyl nitrite (45)	716-999	60, 130, 250	0.5%, 1%, 2%

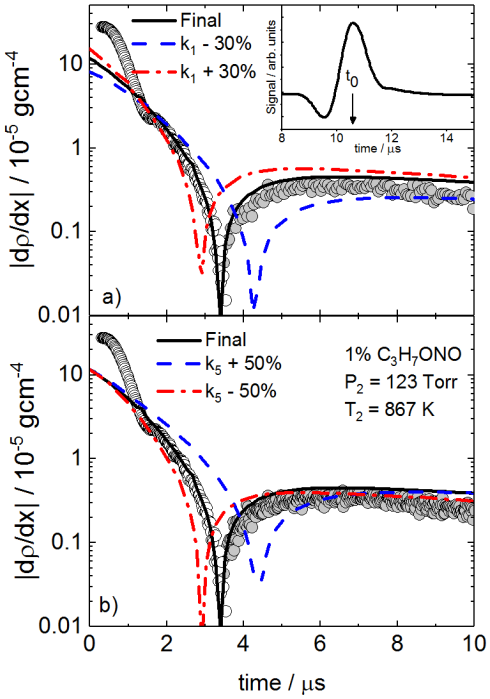

Fig. 1. Example raw LS signals (inset), absolute density gradients (main panels, points), and modeling results (main panels, lines). Open circles positive dρ/dx and shaded circles representing negative dρ/dx. Panel a) shows the sensitivity to $k_{1,C3H7ONO}$ and panel b) shows the sensitivity to $k_{5,ethyl}$.

3. Results and discussion

Approximately 150 experiments were performed at the conditions summarized in Table 2. The experimental conditions and derived rate coefficients for each experiment are given in Tables S2-S4. The LS profiles from the different nitrites at similar T_2 and P_2 look very similar and a typical signal that illustrates the salient features is shown in Fig. 1. The flat region at early times in the raw signal, Fig. 1 inset, is used to establish a baseline. The characteristic valley and peak around 10 µs in the raw profile are due to deflection of the laser beam by the shock wave. The start of chemical reaction, time t_0, occurs within the peak and is located with a well-established method [6] with an accuracy of <0.2 µs. The decaying signals to the right of the large peaks result from chemical reactions. The main panel in Fig. 1 shows a semi-log plot of the absolute density gradients calculated from the raw LS signal. The first several rapidly falling points result from the shock wave/laser beam interaction, which obscures the

chemical signal for ~1 μs. The remaining signal can be interpreted by considering the generic mechanism in Table 1. At early times, the density gradient is positive, indicating the prominence of endothermic reactions, particularly the dissociation of the parent nitrite and the resulting alkoxy radical. As reaction progresses, the density gradients become increasingly negative because the parent nitrite is consumed and exothermic secondary reactions, radical combination and disproportionation, become dominant. The raw LS signals and derived density gradient profiles for each nitrite look very similar because the principle reactions have similar enthalpies and rates of reaction regardless of whether R is ethyl, n-propyl or i-propyl. Furthermore, over the majority of the temperature range of these experiments the rate of dissociation of the alkyl radicals is slow compared to the rates of their recombination and dissociation reactions, and makes little contribution.

Also shown in Fig. 1 are results from simulations calculated via a modeling code based on the methodology of Gardiner et al. [17] and a chemical kinetic mechanism (Table S1). All reactions were treated as reversible, and reverse rates were determined from equilibrium constants and detailed balance. Thermodynamic data for most species were taken from Goos et al. [18], with a few exceptions. For the nitrites, thermodynamic properties were calculated by group additivity with Reaction Mechanism Generator [19]. For NO, H_2CO, CH_3, and C_2H_6 the data are from Active Thermochemical Tables, version 1.122 [20]. For reactions with pressure dependent rate coefficients, appropriate Arrhenius expressions were calculated from literature values. Model development and data fitting were performed iteratively with most rate coefficients fixed to their literature values or adjusted within stated uncertainties, see Table S1. At t_0 the only reaction is dissociation of the nitrite and k_1 was obtained from $d\rho/dx$ at t_0 from the simulations which were fitted to the early part of the profile by adjusting k_1. Additional mechanistic and kinetic parameters were obtained by simulation of the complete density gradient profile.

In the subsections below, results for each of the nitrites are discussed individually, including specific model development for the dissociation of each nitrite and subsequent secondary chemistry. Throughout the discussion, reaction numbers refer to Table 1 and subscripts specifying the relevant alkyl radical, R, or nitrite. The uncertainties in k_1, dissociation of the alkyl nitrite, and k_5, recombination of the alkyl radicals, from the LS experiments are estimated at 30% and 50%, respectively, for each set of experiments.

3.1 n-Propyl nitrite

The initial step in n-propyl nitrite dissociation is cleavage of the O-NO bond to produce a propoxy radical and NO. Curran et al. [21] estimated rate coefficients for dissociation of propoxy to $H_2CO + C_2H_5$ and H + propanal. However, over the experimental range the rate of the propanal channel is 60 to 400 times slower than the C_2H_5 path and is thus negligible. Ethyl radical decomposes by reaction 4 and $k_{4,ethyl}$, varies from $<10^2 - 10^4$ s^{-1} for 700<T<950 K [22]. Consequently, except at the highest temperatures H-atom concentrations are too low for their subsequent reactions to be important. Any H-atoms formed mainly react with C_2H_5, reactions 7 and 8. In principle, H-atoms could react with propyl nitrite, however the bimolecular rates are low due to small concentrations of one or both species. The secondary chemistry of C_3H_7ONO pyrolysis in these experiments is almost entirely dominated by recombination and disproportionation of ethyl radicals, reactions 5 and 6, respectively. Initial estimates of $k_{5,ethyl}$ were taken from Klippenstein et al. [23], who calculated $k_{5,ethyl}$ by variable reaction coordinate transition state theory with an uncertainty of ~30% (S. J. Klippenstein, personal communication, 2017). For the disproportionation reaction, $k_{6,ethyl}$ was obtained from the branching ratio, BR, $k_{5,ethyl}/(k_{5,ethyl}+k_{6,ethyl})=0.86$ [24,25].

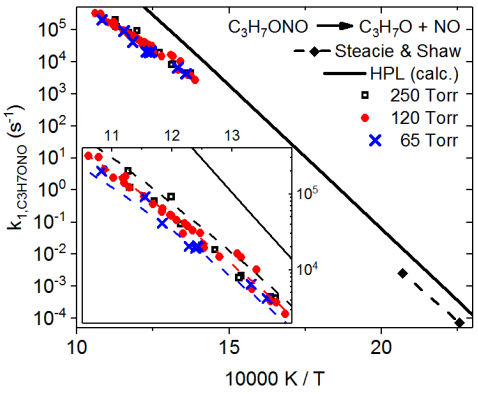

Fig. 2. Arrhenius plots of $k_{1,C3H7ONO}$. LS results (symbols) and RRKM/ME calculations (lines). Also shown are results from [26] at 443 < T < 483K.

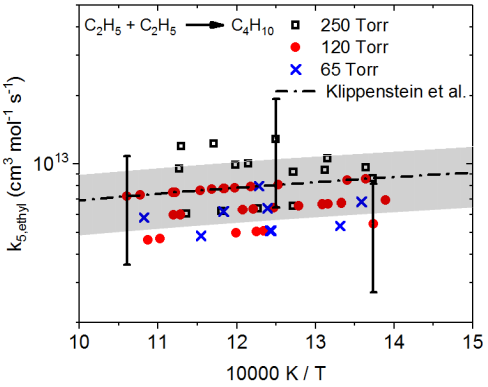

Fig. 3. Arrhenius plot of $k_{5,ethyl}$ (symbols). Calculations by Klippenstein et al. (line) [23]. The shaded area represents the uncertainty in the Klippenstein et al. rate of 30%.

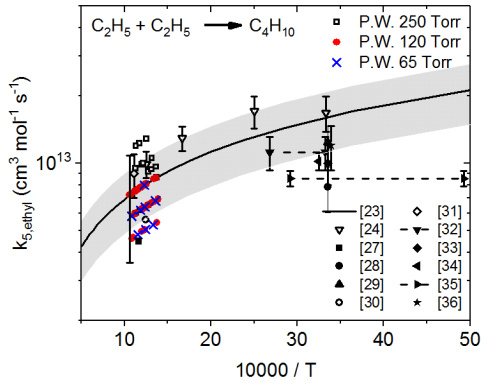

Fig. 4. Comparison $k_{5,ethyl}$ from this work and selected literature values [23,24,27–36]. The shaded area represents the 30% uncertainty in $k_{5,ethyl}$ from [23].

The early part of the simulations are predominantly sensitive to $k_{1,C3H7ONO}$ and the results of sensitivity analyses are shown in Fig. 1a. At later times the simulations are most sensitive to $k_{5,ethyl}$, Fig. 1b. Little sensitivity is observed to $k_{6,ethyl}$ mainly due to the small BR. Consequently, $k_{1,C3H7ONO}$ and $k_{5,ethyl}$ were adjusted to best fit the experimental signal while keeping BR=0.86. From the simulated density gradients at t_0 values of $k_{1,C3H7ONO}$ for n-propyl nitrite dissociation were obtained. Figure 2 shows the experimental $k_{1,C3H7ONO}$ along with $k_{5,ethyl}$ from Steacie and Shaw [26]. The experimental results are very well reproduced by the current RRKM/ME calculations, Fig. 2. The calculated high-pressure limit (HPL) expression is $k_{1,C3H7ONO} = (5.69\pm1.71)\times10^{21}T^{-1.60}\exp(-21458/T)$ s^{-1}. Figure 3 shows an Arrhenius plot of $k_{5,ethyl}$ and a comparison with the theoretical results from [23]. The band represents the 30% uncertainty in the calculation. The agreement between theory and experiment is very good. In Fig. 4 the current results for $k_{5,ethyl}$ are compared with the literature. The current work extends the experimental data to higher temperatures and pressures and supports the falloff predicted by theory [23] and observed by Shafir et al. [24].

3.2 n-Butyl nitrite

Analogous to n-propyl nitrite, dissociation of n-butyl nitrite results in formation of the n-propyl radical (n-C_3H_7), reactions 1 and 2. The secondary chemistry is largely dominated by reactions 5 and 6 but complicated by dissociation of the n-propyl radical. n-C_3H_7 can dissociate by either H-atom elimination, reaction 4, to give propene or by loss of CH_3 to yield ethene, reaction 3. Rate coefficients for reactions -3 and -4 (reverse of reactions 3 and 4, respectively) were calculated from Miller and Klippenstein [37]. These values, in combination with the equilibrium constants, yield $k_{-3,n\text{-}propyl}/k_{-4,n\text{-}propyl}$ of 350-200 ($700<T<950$ K) and $k_{3,n\text{-}propyl} = 10^3 - 10^5$ s^{-1}. Consequently, dissociation of n-propyl and subsequent reactions of methyl are not negligible, particularly for $T_2>\sim850$ K. In this work, abstraction reactions by methyl are not competitive with addition reactions and thus methyl radicals are consumed by reactions 9 and 10 giving butane or ethane, respectively. Reaction 10, CH_3+CH_3,was previously

studied by DFST/LS and k_{10} is taken from reference [38]. An estimate of $k_{9,n\text{-propyl}}$ was obtained by analogy with $CH_3 + C_2H_5=C_3H_8$ [23]. The enthalpies of reactions 5, 9 and 10 are very similar. Thus, the simulations are not sensitive to small errors in the rates of these reactions or reaction 4, n-propyl dissociation. Consequently, $k_{4,n\text{-propyl}}$, $k_{9,n\text{-propyl}}$ and k_{10} were fixed at the literature values.

The reaction of two n-propyl radicals proceeds by both recombination and disproportionation, similar to ethyl. Tsang [39] recommended $k_{5,n\text{-propyl}}/(k_{5,n\text{-propyl}}+k_{6,n\text{-propyl}}) = 0.93$ and this branching fraction was maintained in the modeling. The literature on $k_{5,n\text{-propyl}}$ is very limited. Tsang [39] estimated $k_{5,n\text{-propyl}} = 1\times10^{13}cm^3mol^{-1}s^{-1}$ (300-2500K) which agrees with an experimental value at 298 K by Adachi and Basco [40]. Neither of these capture the expected temperature dependent falloff in $k_{5,n\text{-propyl}}$ and thus initial estimates were made by analogy with C_2H_5 [23]. The simulations were fit to the experimental data by adjusting $k_{1,n\text{-C4H9ONO}}$ and $k_{5,n\text{-propyl}}$.

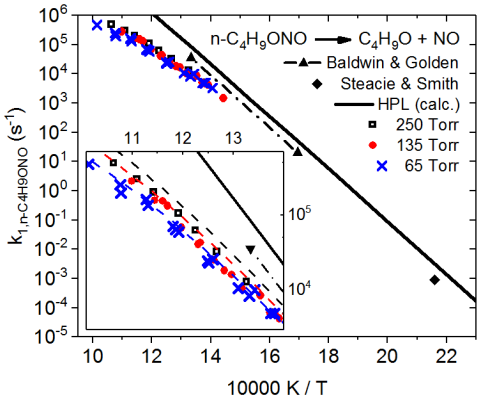

Fig. 5. Arrhenius plots of $k_{1,n\text{-C4H9ONO}}$. LS results (symbols). The HPL of Baldwin and Golden [41] and the experimental point from Steacie and Smith are also shown as well as results from RRKM/ME calculations (lines).

In Fig. 5, $k_{1,n\text{-C4H9ONO}}$ from the present work is shown along RRKM/ME results with values from the literature. The LS data are in falloff and show a small pressure dependence that is very well reproduced by the RRKM/ME calculations. The RRKM/ME calculations yielded a high pressure limit rate coefficient of $k_{1,n\text{-C4H9ONO}} = (9.91\pm2.97)\times10^{21}T^{-1.59}\exp(-21588/T)\ s^{-1}$. Steacie and Smith reported $k_{1,n\text{-}}$

$_{C4H9ONO}$ = 8.88×10^{-4} s^{-1} at 463 K [42]. Baldwin and Golden also studied the decomposition of n-butyl nitrite from 590-750 K using very low pressure pyrolysis [41]. Their RRKM analysis yielded a rate coefficient at the high-pressure limit (HPL) of $k_{1,n\text{-}C4H9ONO}$ = 3.16×10^{16}exp(-20634/T) s^{-1}. Their reported energy of activation (41.0 kcal/mol) is very similar to what is reported in the present work (43.0 kcal/mol). The RRKM/ME HPL is about a factor of 2.5 greater than that from Baldwin and Golden and a similar amount higher than the Steacie and Smith value.

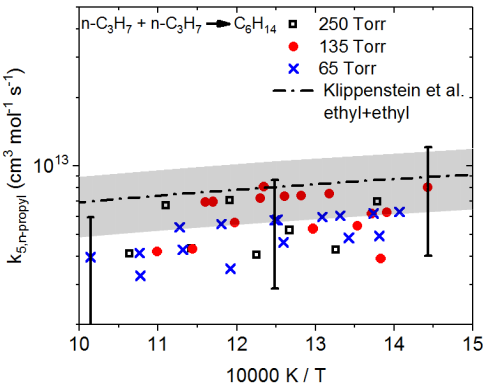

Fig. 6. Arrhenius plot of $k_{5,n\text{-}propyl}$ (symbols). Calculations by Klippenstein et al. for ethyl + ethyl recombination [23]. The shaded area represents the uncertainty in the Klippenstein et al. rate of 30%.

Figure 6 shows the experimental $k_{5,n\text{-}propyl}$. The uncertainties are estimated at 50% and within the scatter of the data there is no discernable pressure dependence. There are no literature values for recombination of n-propyl radicals and for comparison $k_{5,ethyl}$ from Klippenstein et al. [23] are shown. The $k_{5,n\text{-}propyl}$ consistently lie lower than $k_{5,ethyl}$ which would be expected as the general trend is for recombination rate coefficients to decrease with increasing molecular size.

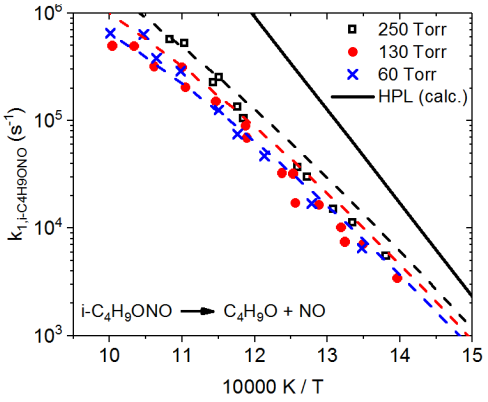

Fig. 7. Arrhenius plots of $k_{1,i\text{-}C4H9ONO}$. LS results (symbols) and RRKM/ME calculations (lines).

3.3 iso-Butyl nitrite

The model development for iso-butyl nitrite pyrolysis was carried out similarly to the previously discussed nitrites and reaction 1 produces i-butoxy and NO. The experimental $k_{1,i\text{-}C4H9ONO}$ are shown in Fig. 7 along with results from RRKM/ME calculations, which yielded a high-pressure limit rate coefficient of $k_{1,i\text{-}C4H9ONO} = 3.92\pm1.18\times10^{21}T^{-1.58}\exp(-21162/T)\ s^{-1}$. The experimental points are in falloff and show a small but well-defined pressure dependence that is captured by the theoretical model.

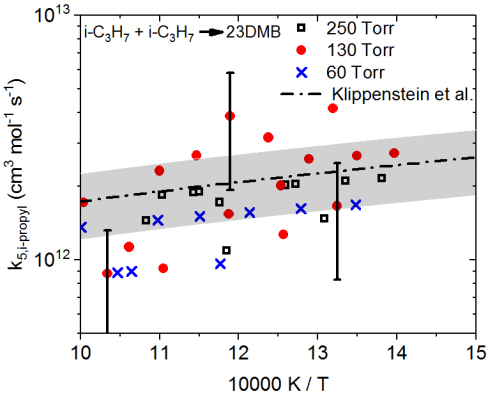

Fig. 8. Arrhenius plot of $k_{5,i\text{-propyl}}$ (symbols). Calculations by Klippenstein et al. [23]. The shaded area represents the uncertainty in the Klippenstein et al. rate of 30%.

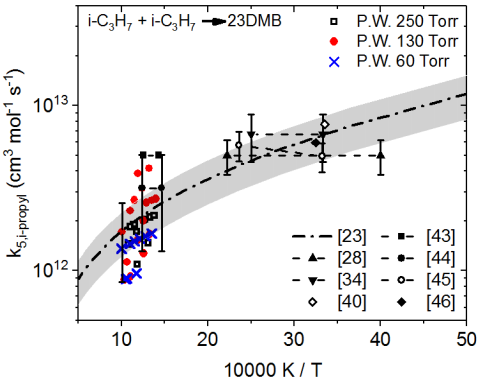

Fig. 9. Comparison of $k_{5,i\text{-propyl}}$ from the present work and selected literature results [28,34,43–45,40,46]. The shaded area represents the uncertainty in the Klippenstein et al. [23] rate of 30%.

i-Propyl radicals are formed via reactions 1 and 2. Similar to C_2H_5 they dissociate by elimination of H, reaction 4, and $k_{4,i\text{-propyl}}$ increases from 10^2 s^{-1} to 2×10^4 s^{-1} (700<T<950K) [37]. Thus, apart from at the highest temperatures, reaction 4 is negligible. Any H-atoms created react by addition to i-C_3H_7 producing propane, reaction 7. The rate coefficient, $k_{7,i\text{-propyl}}$, was obtained from Harding et al. [47] and that for the disproportionation channel, reaction 8, was taken from Tsang [39]. Under all condition studied $k_{7,i\text{-propyl}}/k_{8,i\text{-propyl}}$ >100. i-Propyl radicals mainly react by recombination, reaction 5, and initial values $k_{5,i\text{-propyl}}$ were obtained from Klippenstein et al. [23]. Following the recommendation of Tsang [39] the BR to the disproportionation channel was set as $k_{5,i\text{-propyl}}/(k_{5,i\text{-propyl}}+k_{6,i\text{-propyl}})=0.6$. The final $k_{5,i\text{-propyl}}$ are shown in Fig. 8, and comparison to other studies from the literature are shown in Fig. 9. The uncertainties in $k_{5,i\text{-propyl}}$ are estimated as 50%. Similar to $k_{5,ethyl}$ and $k_{5,n\text{-propyl}}$ no pressure dependence is observed within the scatter of the data. However, the rate coefficients do follow the general temperature dependent falloff shown by the theoretical results of Klippenstein et al [23]. Similar to the results found for ethyl and n-propyl radicals the current work extends the experimental data to higher temperatures and shows good agreement with the theoretical models.

4. Summary

Experimental results on the dissociation of n-propyl nitrite, n-butyl nitrite, and iso-butyl nitrite, in the temperature range of approximately 700-1000 K at pressures between 60-260 Torr were presented and their use as clean radical sources was discussed. Chemical kinetic models were developed for each of the nitrite species in order to simulate the experimental data, which include dissociation of the parent nitrite and the resulting alkoxy radical and secondary chemistry involving the alkyl radical produced. These experiments demonstrate the use of nitrites as radical precursors in combustion experiments in a temperature range where radical combination and disproportionation reactions are competitive with radical dissociation reactions, and therefore provide a convenient means to study these processes.

5. Acknowledgements

This work was performed under the auspices of the Office of Basic Energy Sciences, Division of Chemical Sciences, Geosciences, and Biosciences, U.S. Department of Energy, under contract number DE-AC02-06CH11357. MEF and CFG gratefully acknowledge support from the U.S. National Science Foundation through Award Number CBET-1553366.

6. References

[1] R.S. Tranter, A.W. Jasper, J.B. Randazzo, J.P.A. Lockhart, J.P. Porterfield, Proc. Combust. Inst. 36 (2017) 211–218.

[2] L. Batt, K. Christie, R.T. Milne, A.J. Summers, Int. J. Chem. Kinet. 6 (1974) 877–885.

[3] R.S. Tranter, B.R. Giri, Rev. Sci. Instrum. 79 (2008) 94103.

[4] J.B. Randazzo, R.S. Tranter, Rev. Sci. Instrum. 86 (2015) 16117.

[5] J.H. Kiefer, in:, A. Lifshitz (Ed.), Shock Waves Chem., Marcel Dekker, New York, 1981.

[6] J.H. Kiefer, Z. Al-Alami, J.-C. Hajduk, Appl. Opt. 20 (1981) 221–230.

[7] W.C. Gardiner, Y. Hidaka, T. Tanzawa, Combust. Flame 40 (1981) 213–219.

[8] R. Peverati, D.G. Truhlar, J. Phys. Chem. Lett. 2 (2011) 2810–2817.

[9] S.J. Klippenstein, L.B. Harding, B. Ruscic, J. Phys. Chem. A 121 (2017) 6580–6602.

[10] M. J. Frisch, G. W. Trucks, H. B. Schlegel, G. E. Scuseria, M. A. Robb, J. R. Cheeseman, G. Scalmani, V. Barone, B. Mennucci, G. A. Petersson, H. Nakatsuji, M. Caricato, X. Li, H. P. Hratchian, A. F. Izmaylov, J. Bloino, G. Zheng, J. L. Sonnenberg, M. Hada, M. Ehara, K. Toyota, R. Fukuda, J. Hasegawa, M. Ishida, T. Nakajima, Y. Honda, O. Kitao, H. Nakai, T. Vreven, J. A. Montgomery (Jr), J. E. Peralta, F. Ogliaro, M. Bearpark, J. J. Heyd, E. Brothers, K. N. Kudin, V. N. Staroverov, R. Kobayashi, J. Normand, K. Raghavachari, A. Rendell, J. C. Burant, S. S. Iyengar, J. Tomasi, M. Cossi, N. Rega, J. M. Millam, M. Klene, J. E. Knox, J. B. Cross, V. Bakken, C. Adamo, J. Jaramillo, R. Gomperts, R. E. Stratmann, O. Yazyev, A. J. Austin, R. Cammi, C. Pomelli, J. W. Ochterski, R. L. Martin, K. Morokuma, V. G. Zakrzewski, G. A. Voth, P. Salvador, J. J. Dannenberg, S. Dapprich, A. D. Daniels, A. Farkas, J. B. Foresman, J. V. Ortiz, J. Cioslowski and D. J. Fox, GAUSSIAN09, Revision E.01, Gaussian Inc. Wallingford CT.

[11] Y. Georgievskii, J.A. Miller, M.P. Burke, S.J. Klippenstein, J. Phys. Chem. A 117 (2013) 12146–12154.

[12] S. J. Klippenstein, A. W. Jasper, J. A. Miller and Y. Georgievskii, PAPR: Predictive Automated Phenomenological Rates, available at http://tcg.cse.anl.gov/papr/.

[13] J.O. Hirschfelder, E. Wigner, J. Chem. Phys. 7 (1939) 616–628.

[14] W.H. Miller, J. Chem. Phys. 65 (1976) 2216–2223.

[15] W.J. Chesnavich, L. Bass, T. Su, M.T. Bowers, W.J. Chesnavich, L. Bass, T. Su, M.T. Bowers, J. Chem. Phys. 74 (1981) 2228–2246.

[16] A.D. Danilack, C.F. Goldsmith, Proc. Combust. Inst. Submitted (2017).

[17] W.C. Gardiner, B.F. Walker, C.B. Wakefield, in:, A. Lifshitz (Ed.), Shock Waves Chem., Marcel Dekker, New York, 1981.

[18] E. Goos, A. Burcat and B. Ruscic, Extended Third Millenium Thermodynamic Database for Combustion and Air-Pollution use with updates from Active Thermochemical Tables. http://garfield.chem.elte.hu/Burcat/THERM.DAT.; Last Print Edition: Burcat, A.; Ruscic, B. Third Millenium Ideal Gas and Condensed Phase Thermochemical Database for Combustion with updates from Active Thermochemical Tables. Argonne National Laboratory, Argonne, Illinois, U.S.A. and Technion-IIT, Haifa, Israel, Report ANL-05/20 and TAE 960, 2005.

[19] W.H. Green, R.H. West, RMG - Reaction Mechanism Generator, <rmg.mit.edu> (2017).

[20] B. Ruscic and D. H. Bross, Active Thermochemical Tables (ATcT) values based on ver. 1.122 of the Thermochemical Network (2016); available at ATcT.anl.gov.

[21] H.J. Curran, Int. J. Chem. Kinet. 38 (2006) 250–275.

[22] X. Yang, R.S. Tranter, Int. J. Chem. Kinet. 44 (2012) 433–443.

[23] S.J. Klippenstein, Y. Georgievskii, L.B. Harding, Phys. Chem. Chem. Phys. 8 (2006) 1133–1147.

[24] E. V Shafir, I. Slagle, V.D. Knyazev, J. Phys. Chem. A 107 (2003) 6804–6813.

[25] D.L. Baulch, C.T. Bowman, C.J. Cobos, R.A. Cox, T. Just, J.A. Kerr, M.J. Pilling, D. Stocker, J. Troe, W. Tsang, R.W. Walker, J. Warnatz, J. Phys. Chem. Ref. Data 34 (2005) 757–1397.

[26] E.W.R. Steacie, G.T. Shaw, J. Chem. Phys. 3 (1935) 344–347.

[27] D.M. Golden, K.Y. Choo, M.J. Perona, L.W. Piszkiewicz, Int. J. Chem. Kinet. 8 (1976) 381–387.

[28] D.A. Parkes, C.P. Quinn, J. Chem. Soc., Faraday Trans. 1 72 (1976) 1952–1971.

[29] H. Adachi, N. Basco, D.G.L. James, Int. J. Chem. Kinet. 11 (1979) 995–1005.

[30] S. Corbel, P.-M. Marquaire, G.-M. Come, Chem. Phys. Lett. 80 (1981) 2–4.

[31] P.D. Pacey, J.H. Wimalasena, J. Phys. Chem. 88 (1984) 5657–5660.

[32] N.L. Arthur, J. Chem. Soc., Faraday Trans. 2 82 (1986) 1057–1065.

[33] J. Munk, P. Pagsberg, E. Ratajczak, A. Sillesen, J. Phys. Chem. 90 (1986) 2752.

[34] C. Anastasi, N.L. Arthur, J. Chem. Soc. Farady Trans. 83 (1987) 277–287.

[35] O. Dobis, S.W. Benson, J. Am. Chem. Soc. 113 (1991) 6377–6386.

[36] D.B. Atkinson, J.W. Hudgens, J. Phys. Chem. A 101 (1997) 3901–3909.

[37] J.A. Miller, S.J. Klippenstein, J. Phys. Chem. A 177 (2013) 2718–2727.

[38] X. Yang, A.W. Jasper, J.H. Kiefer, R.S. Tranter, J. Phys. Chem. A 113 (2009) 8318–8326.

[39] W. Tsang, J. Phys. Chem. Ref. Data 17 (1988) 887–951.

[40] H. Adachi, N. Basco, Int. J. Chem. Kinet. 13 (1981) 367–384.

[41] A.C. Baldwin, D.M. Golden, Chem. Phys. Lett. 60 (1978) 7–10.

[42] E.W.R. Steacie, W.M. Smith, J. Chem. Phys. 4 (1936) 504–507.

[43] D.M. Golden, G.N. Spokes, S.W. Benson, Angew. Chemie Int. Ed. English 12 (1973) 534–546.

[44] D.M. Golden, Z.B. Alfassi, P.C. Beadle, Int. J. Chem. Kinet. 6 (1974) 359–370.

[45] P. Arrowsmith, L.J. Kirsch, J. Chem. Soc. - Faraday Trans. 1 74 (1978) 3016–3021.

[46] N.L. Arthur, C. Anastasi, Bull. Des Soc. Chemiques Belges 92 (1983) 647.

[47] L.B. Harding, Y. Georgievskii, S.J. Klippenstein, J. Phys. Chem. A 109 (2005) 4646–4656.

7. Supplemental material

This article is accompanied by supplemental material, which includes a full reaction table for all four nitrites (Table S1), a full list of experimental temperatures, pressures, and rate coefficients for nitrite dissociation and alkyl radical recombination (Tables S2-S4), the propyl nitrite synthesis procedure, and infrared (IR; Fig. S1, and nuclear magnetic resonance (NMR; Figs. S2-S4) of n-propanol (reactant) and n-propyl nitrite (product).

List of figure captions

Fig. 1. Example raw LS signals (inset), absolute density gradients (main panels, points), and modeling results (main panels, lines). Open circles positive dρ/dx and shaded circles representing negative dρ/dx. Panel a) shows the sensitivity to $k_{1,C3H7ONO}$ and panel b) shows the sensitivity to $k_{5,ethyl}$.

Fig. 2. Arrhenius plots of $k_{1,C3H7ONO}$. LS results (symbols) and RRKM/ME calculations (lines). Also shown are results from [26] at 443 < T < 483K.

Fig. 3. Arrhenius plot of $k_{5,ethyl}$ (symbols). Calculations by Klippenstein et al. (line) [23]. The shaded area represents the uncertainty in the Klippenstein et al. rate of 30%.

Fig. 4. Comparison $k_{5,ethyl}$ from this work and selected literature values [23,24,27–36]. The shaded area represents the 30% uncertainty in $k_{5,ethyl}$ from [23].

Fig. 7. Arrhenius plots of $k_{1,i\text{-}C4H9ONO}$. LS results (symbols) and RRKM/ME calculations (lines).

Fig. 8. Arrhenius plot of $k_{5,i\text{-}propyl}$ (symbols). Calculations by Klippenstein et al. [23]. The shaded area represents the uncertainty in the Klippenstein et al. rate of 30%.

Fig. 9. Comparison of $k_{5,i\text{-}propyl}$ from the present work and selected literature results [28,34,43–45,40,46]. The shaded area represents the uncertainty in the Klippenstein et al. [23] rate of 30%.